# Investigation of fuel cells using scanning neutron imaging and a focusing neutron guide

C. Tötzke[a,c,*], I. Manke[a], T. Arlt[a], H. Markötter[a], N. Kardjilov[a], A. Hilger[a,c], S. Williams[a], P. Krüger[b], R. Kuhn[b], C. Hartnig[b,1], J. Scholta[b], and J. Banhart[a,c]


[a] *Helmholtz-Zentrum Berlin (HZB), 14109 Berlin, Germany*
 *Zentrum für Sonnenenergie- und Wasserstoff-Forschung Baden-Württemberg (ZSW),*
 *89081 Ulm, Germany*
[c] *Technische Universität Berlin, 10623 Berlin, Germany*


[*] *corresponding author. Fon: +49 30 8062 42615*
                        *Email:* christian.toetzke@helmholtz-berlin.de

[1] *present address: Chemetall GmbH, Trakehner Straße 3, 60487 Frankfurt a. M.*

## Abstract

We present two different methods to increase the size of available neutron beams in order to allow for the investigation of large objects. Application of these methods is demonstrated for radiographic imaging of fuel cells. The first approach is a scanning procedure based on the coordinated translation of detector and sample through the beam. Further advancement was achieved by installing a focusing neutron guide which offers an expanded neutron beam size after diverging from a focused point source.

## Key words

neutron imaging; fuel cells; neutron focusing guide; water management; water distribution


## 1. Introduction

The performance, durability and successful operation of fuel cells rely essentially on an effective water management. For this reason, the evaluation of the water distribution in operating fuel cells is one of the key issues in fuel cell research [1-6].

Imaging methods have been established as valuable tools to study media distributions *in situ* [7-8]. Numerous studies were published reporting on successful applications of neutron imaging [9-25], x-ray imaging [26-31] and magnetic resonance imaging [32-34] to address various problems of fuel cells research. Neutron imaging is the technique most appropriate to visualize the water distribution inside entire cells.

The investigation of large fuel cells is especially interesting for industrial applications, where fuel cell dimensions range up to one meter, but sample sizes are limited by the cross-sectional area of the available neutron beam. Here, we present two ways to overcome insufficient beam size in order to investigate very large fuel cells.

## 2. Technical details

### 2.1. Neutron imaging facility

The experiments were performed at the V7 CONRAD instrument of the Helmholtz-Zentrum Berlin (HZB) [35]. The imaging facility is placed at the end of the curved neutron guide NL1b facing the cold neutron source of the Hahn-Meitner research reactor BER-II. The $^{58}$Ni coated neutron guide provides a flux density of $2 \cdot 10^8$ n/(cm$^2$s); while the curvature (radius $\approx$ 3000 m) keeps the noise created by thermal neutrons and gamma radiation to a low level. A pinhole is used to collimate the beam. A pinhole exchanger provides different diameters, namely 1, 2, and 3 cm. The distance between the pinhole and the downstream sample position is 5 m resulting in beam collimation rates L/D of 521, 261, 174, and neutron fluxes of $5.8 \times 10^6$, $1.6 \times 10^7$, and $2.4 \times 10^7$ n/(cm$^2$s), respectively.

### 2.2. Fuel cells

A single cell setup with a size of $14 \times 14$ cm$^2$ and an active area of 100 cm$^2$ was studied. The test cell investigated by using the scanning option was equipped with fivefold anodic and threefold cathodic serpentine flowfield which had 1 mm wide channels and ribs machined in separate blank composite plates. A Gore 5761 membrane electrode assembly (MEA) was used and the carbon fiber material SGL 10BB was used as gas diffusion layer (GDL).

The test cell investigated by using the elliptical neutron guide set up was equipped with a threefold anodic and cathodic flowfield, respectively. A Gore 5761 was used as MEA. The GDL at the anode side was SGL 10BB, whereas the cathodic side was equipped with two different GDLs: SGL 10FC at the left and SGL 10CC at the right half.

## 3. Results

The CONRAD instrument provides an overall beam size of about $12 \times 12$ cm$^2$. However, the beam intensity is not uniformly distributed. While at the beam centre an area of about $7 \times 7$ cm$^2$ offers high intensity, the neutron flux decreases strongly towards the beam edges by one order of magnitude [36].

When large samples are investigated, the inhomogeneous intensity distribution results in unfavorable image characteristics away from the high flux density available in center of the beam. Neutron imaging is dominated by "shot noise" resulting from statistical fluctuations in the finite number of neutrons detected, as defined in a Poisson distribution. The value of the standard deviation of the noise is given as the square root of the signal (the number of neutrons recorded, N). Thus, the signal-to-noise ratio (SNR) is defined as $N/\sqrt{N}$, which is reduced to simply $\sqrt{N}$. A high recorded neutron signal in a given area will produce a high SNR, as in the center of the neutron imaging beam, while a low neutron signal creates low image quality, observed at the edges of the beam. This fundamental aspect of imaging quality is often referred to simply as "signal statistics" or "neutron statistics".

This problem is illustrated using the example of a fuel cell with the dimensions of $14 \times 14$ $cm^2$ and an active area of $10 \times 10$ $cm^2$. Figure 1 shows a radiographic image of the cell and the corresponding flat-field. While exposure time is correctly adjusted with respect to the image centre, the surrounding area exhibits a low neutron signal. The intensity line plots provided in Figure 2 show that compared to the image centre the intensity at the edges is lower by one order of magnitude. Prolongation of exposure time is no option to improve the signal statistics, due to the inherent restriction imposed by saturation of the 16-bit CCD detection capabilities in the central image area.
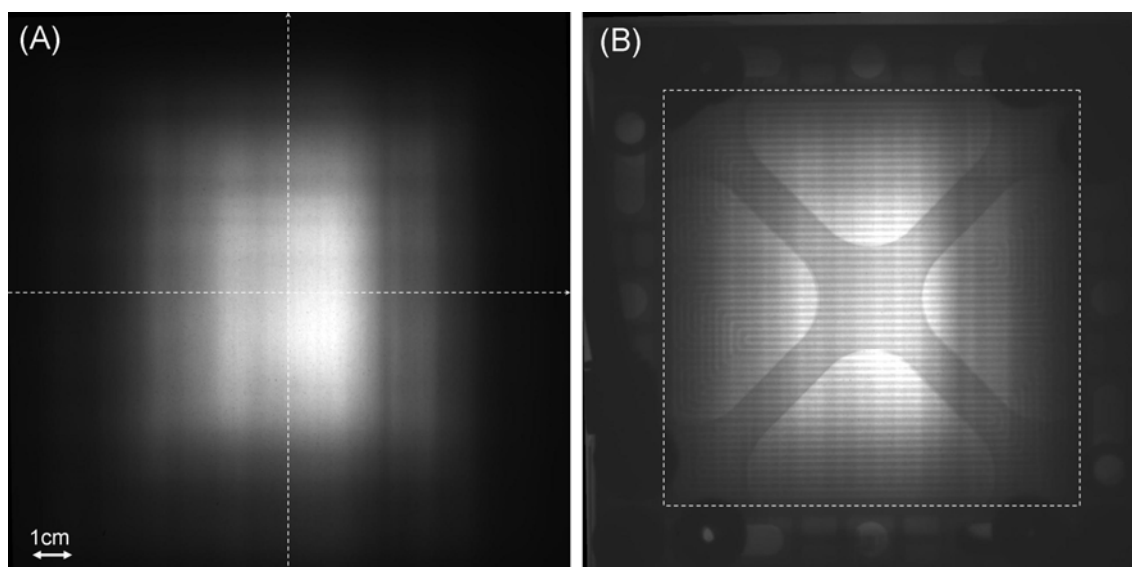


**Figure 1: Neutron radiography of a 14 x 14cm$^2$ PEMFC taken by the standard set up of CONRAD instrument. A) beam profile (flat-field) and B) raw image of the test cell (active area bordered by the dashed line), exposure time 60 s.**
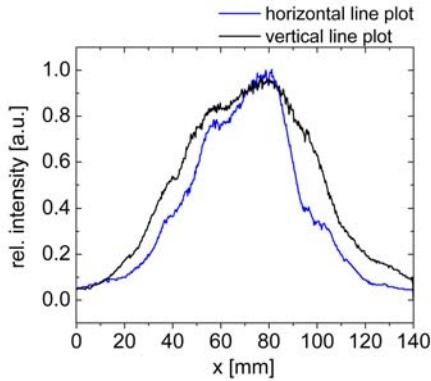
**Figure 2: Intensity line plots through the flat-field image centre along the dashed arrows drawn in figure 1 A.**

The problem can be addressed by applying a scanning procedure: Sample and detector are firmly fixed to each other, and are translated together through the beam in perpendicular to the direction of beam propagation. Figure 3 shows the principle of image acquisition. Each acquisition comprises a complete scan, i.e. within the exposure time the sample detector assembly is translated all the way through the beam. As a result, high neutron intensity is distributed horizontally across the image. The quality of the images obtained by this procedure crucially relies on the firm attachment of sample and detector since any movement relative to one another would result in motion blur, thus negatively affecting image resolution.
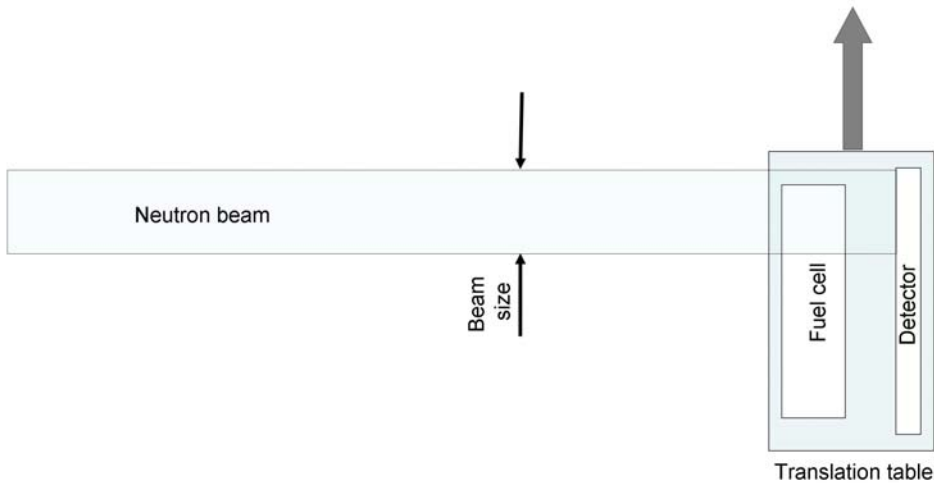


**Figure 3: Principle set up for the scanning procedure.**

The scanning technique was successfully applied to *in situ* radiographic investigations of polymer electrolyte membrane fuel cells (PEMFC). Figure 4 shows the radiogram of the test cell and the corresponding flat-field obtained by employing the scanning option. Compared to the image obtained by the standard setup (Figure 1) (without scanning), the quality

improvement regarding the intensity distribution is obvious. Images obtained by the scanning procedure possess almost uniform intensity in the horizontal direction creating higher quality images with both lower noise and more uniform distribution. The SNR is significantly improved, particularly for the area outside the image centre. Figure 5 shows intensity plots along the dashed vertical and horizontal arrow drawn in Figure 4. As stated above in horizontal direction intensity is distributed almost uniformly. However, in vertical direction intensity is still maximal at the image centre and falls towards the edges.
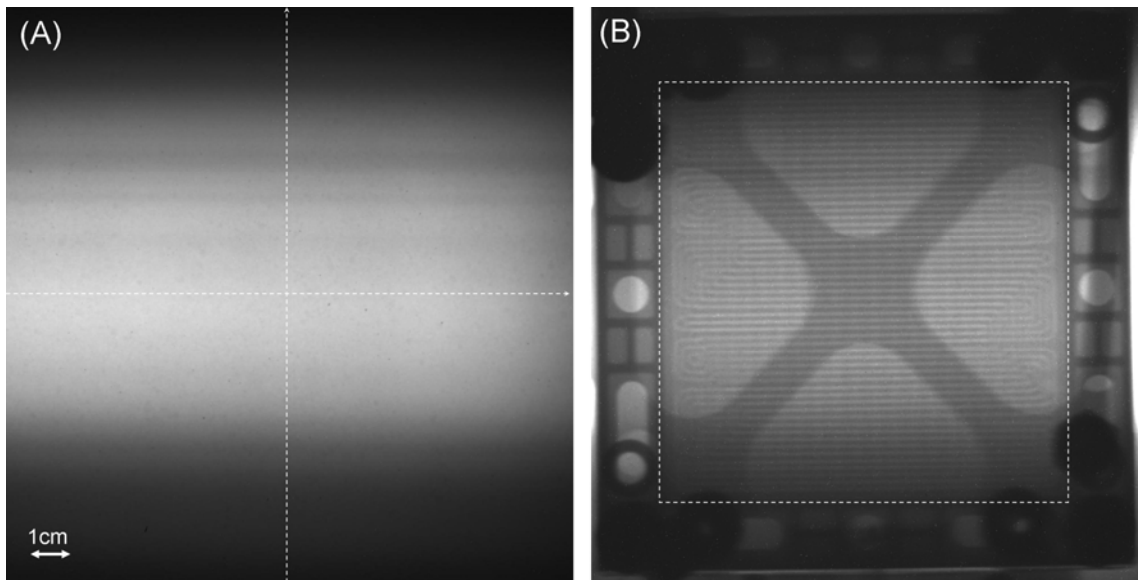


**Figure 4: Neutron radiography of a 14 x 14cm$^2$ PEMFC taken by using the scan option: A) beam profile (flat-field) and B) raw image of the test cell (active area bordered by the dashed line), exposure time 60 s.**
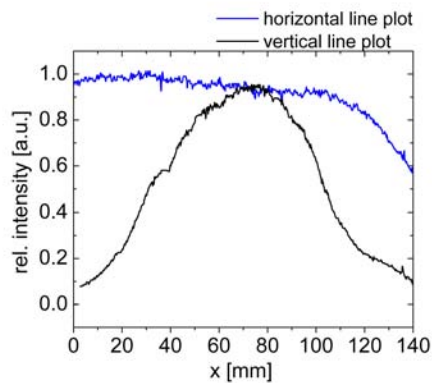


**Figure 5: Intensity line plots through the flat-field image centre along the dashed arrows drawn in figure 4 A.**

Taking advantage of the improved signal statistics, the *in situ* water distribution in the fuel cell can be visualized. Figure 6 documents the water accumulation in the test cell during a 20-minute start up process where the temperature increases from 20 to 60°C. All images are

normalized with respect to the dry reference state. While the current density is kept to $500 \, \text{mA/cm}^2$, water accumulates at first in the GDL visible as the dark shade covering the whole active cell area (see e.g. Figure 6 C). Upon saturation of the GDL, water enters the flowfield channels and forms droplets and even larger agglomerations, which are eventually driven out of the cell by the gas streams.
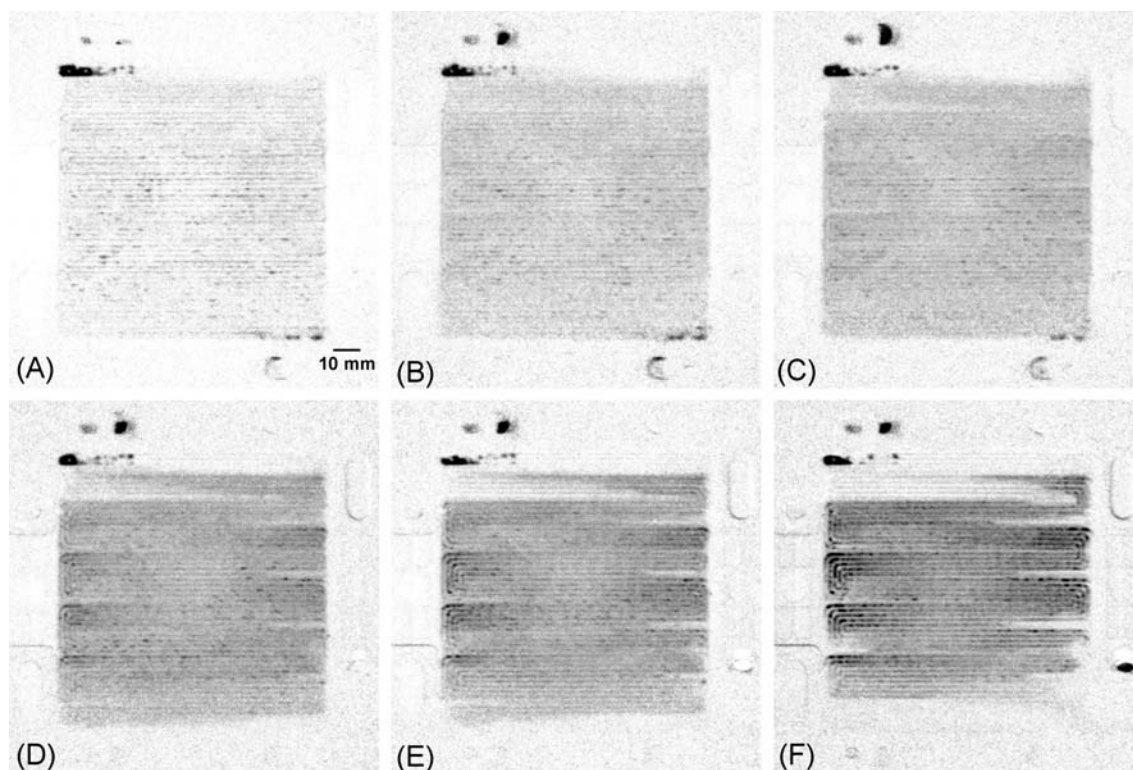


**Figure 6: Series of quotient images showing the water accumulation in the test cell during a 20-min start up. Current density j=500 mA/cm², exposure time 60s: A) t=3 min; B) t=5 min; C) t=9 min; D) t=14 min; E) t=16 min; F) t=20min.**

As demonstrated, the scanning procedure yield images with improved intensity distribution, i.e. uniform intensity in horizontal direction. A desirable advancement would be a homogenous intensity also in vertical direction. In theory, this could be achieved by including an additional vertical scan in the procedure. However, the scanning method is vulnerable to mechanical instability. Translational movements of the sample detector unit can produce vibrations, and subsequent micromotions of sample and/or detector, relative to one another, have a negative impact on the spatial resolution and the image normalization. The introduction of a second, vertical scanning stage would aggravate the problem. Additionally, scanning movement of the fuel cell inevitably entails permanent mechanical interaction with associated supply connections like cables, gas supply, and temperature conditioning hoses.

6

This complicates precise sample positioning and can provoke sample dislocation during the scanning procedures.

Taking into account these drawbacks, an alternative technical strategy was employed to overcome the beam size limitation. The alternative approach is based on the application of a focusing neutron guide which makes scanning procedures unnecessary [37]. Figure 7B illustrates the experimental principle of beam size enlargement with respect to the standard set up of a straight guide (shown in Figure 7A).
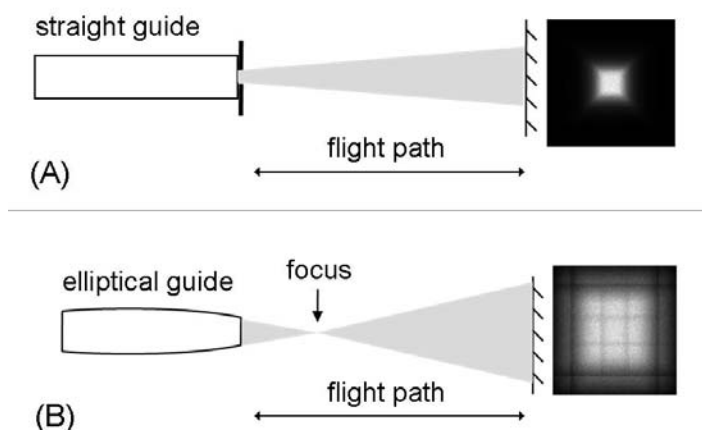


**Figure 7: Illustration of the principal setup: A) standard setup, B) beam enlargement using by means of a focusing guide. Adapted from [38] (with permission from Elsevier).**

The elliptical guide was integrated as an additional optical module of the beamline. It has a length of 500 mm and a rectangular cross sections of $10.6 \times 21.2$ mm$^2$ at the guide entrance and $4 \times 8$ mm$^2$ at the exit. The inner walls have a supermirror coating m=3, with the focal point located 80 mm downstream with respect to the exit of the guide . The distance between the exit of the elliptical guide and the neutron detector was 4.5 m. At this distance, the divergence from the focal point produced by the elliptical guide provides a nearly homogeneously illuminated area of approximately $20 \times 20$ cm$^2$. The observed segments in the image are due to the neutron wavelength distribution, which limits the range of the available total reflection angles and produces discontinuities in the image. Using this configuration, the beam size can be enlarged by a factor of 3 in horizontal and vertical direction [38].

Figure 8 shows the radiogram of a fuel cell and the corresponding flat-field obtained by using the neutron focusing guide. Intensity line plots in horizontal and vertical direction (indicated by dashed arrows in Figure 8 A) are provided with Figure 9. When compared to the scanning

option (Figure 4 and 5) a more homogenous intensity distribution over the whole cell area is achieved. The SNR within the uppermost and lowermost image areas is improved.
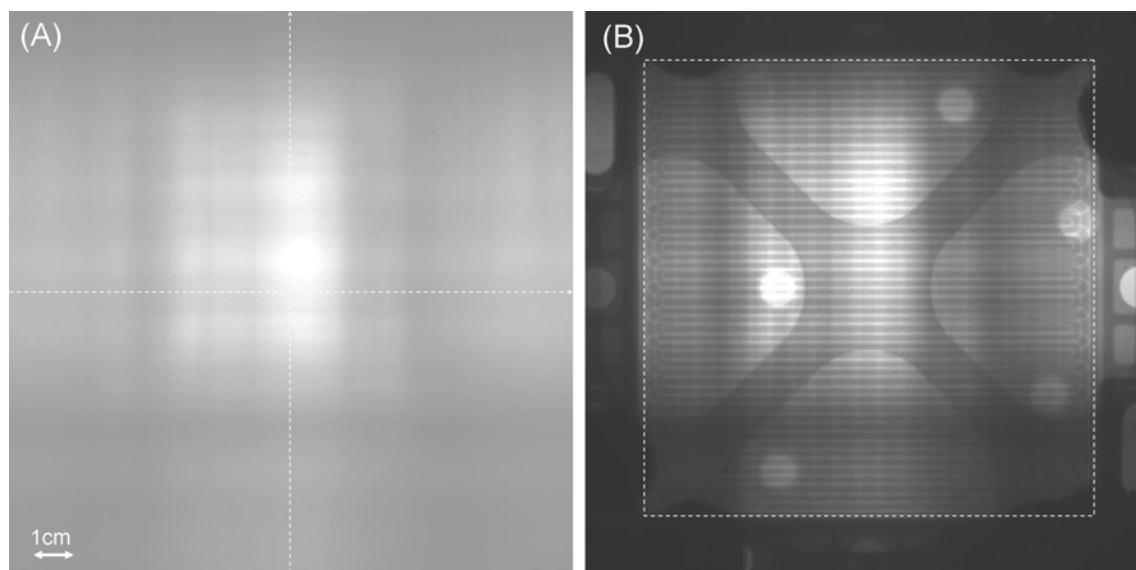


**Figure 8:** **Neutron radiography of a 14 x 14cm$^2$ PEMFC taken by using the focusing guide. A) beam profile (flat-field) and B) raw image of the test cell (active area bordered by the dashed line), exposure time 60s.**
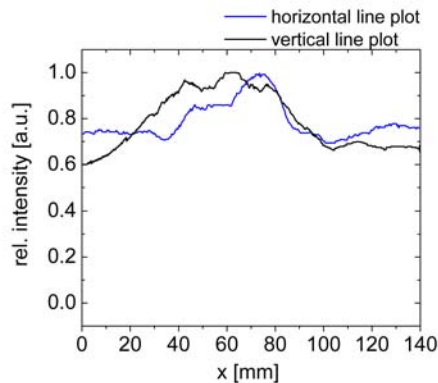


**Figure 9: Intensity line plots through the flat-field image centre along the dashed arrows drawn in figure 8 A.**

The application of the setup is suitable for *in situ* investigations of large fuel cells. An important advantage over the scanning method is the fixed sample position. Thus, the test cell is not subjected to any mechanical agitation originating from scanning movements which could lead to sample dislocation. In Figure 10 an example of water distribution during operation is given. The image series comprises quotient images taken during 3 hours of operation. All images are normalized with respect to the dry cell.
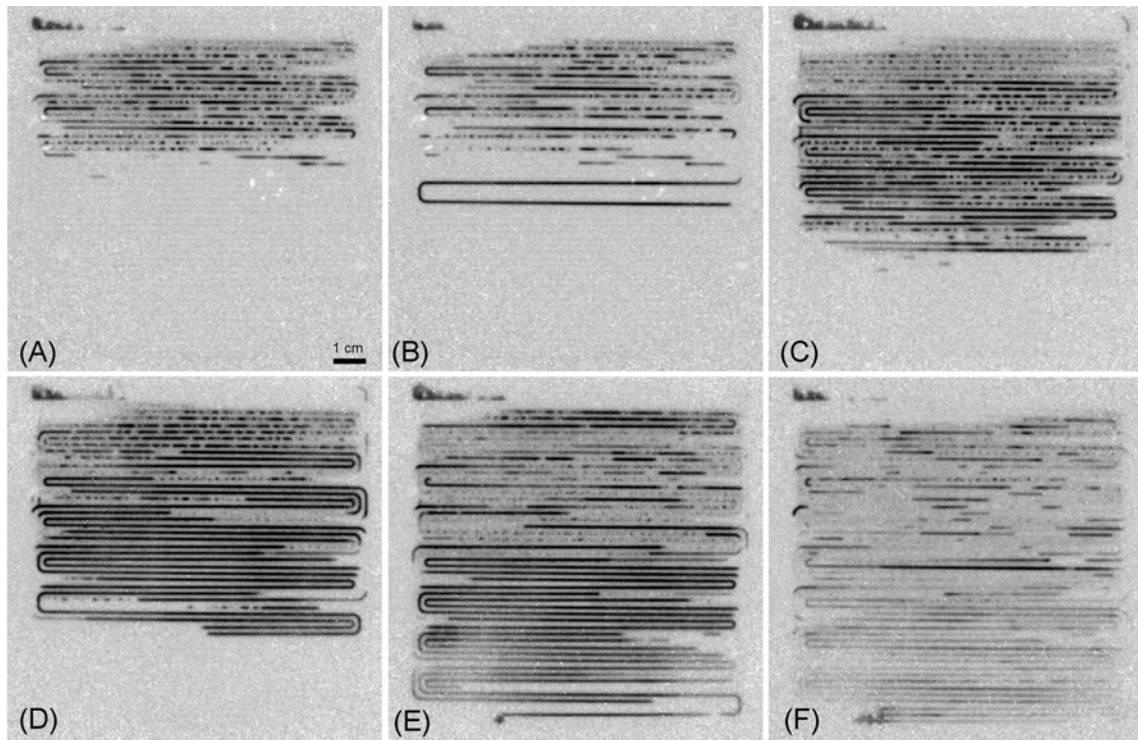
**Figure 10: Series of quotient images revealing the evolution of the water distribution in a fuel cell during 3 hours of operation at current densities ranging from 100 mA/cm2 to 700 mA/cm2, exposure time 60s.**

As in Figure 6, water accumulations are visible within the channel meander. They appear as dark, snake like shapes. Driven by the gas streams these agglomerations proceed towards the outlets (bottom of the images) where they finally exit the cell. In between the flowfield channels, dark shaded areas indicate the water accumulation within the GDLs.


## 4. Conclusions

We presented two different ways to increase the observable cell size for radiographic *in situ* investigations of PEMFC fuel cells. A scanning method based on the concerted movement of both the fuel cell and the detector yields images with a uniform intensity in the horizontal direction. The improved signal statistics allow for a clear visualization of water distributions even at the edges of large fuel cells. However, mechanical instabilities can result in micromotions of the sample relative to the detector which have negative impact on the spatial resolution and data normalization. The installation of the focusing guide is an advanced option to overcome beam size limitations. The intensity distribution is more uniform compared to traditional pinhole collimation or the scanning option, and scanning movements are unnecessary. The improved signal statistics also allow for a quantitative analysis of the

9

water distribution. Thus, the focusing guide is a good solution when beam size has to be increased.

**Acknowledgement**

**References**

[1] L. Carrette, K.A. Friedrich, U. Stimming, Fuel Cells, 1 (2001) 5-39.
[2] C.-Y. Wang, Two-phase flow and transport, in: W. Vielstich, A. Lamm, H.A. Gasteiger (Eds.) Handbook of Fuel Cells – Fundamentals, Technology and Applications, John Wiley & Sons, Chichester, 2003, pp. 337–347.
[3] C.-Y. Wang, Chemical Reviews, 104 (2004) 4727-4766.
[4] S. Litster, N. Djilali, Transport Phenomena in Fuel Cells, in, WIT Press, Southampton UK, 2005, pp. 175-213.
[5] N. Djilali, P.C. Sui, International Journal of Computational Fluid Dynamics, 22 (2008) 115-133.
[6] W. Schmittinger, A. Vahidi, Journal of Power Sources, 180 (2008) 1-14.
[7] I. Manke, H. Markötter, C. Tötzke, N. Kardjilov, R. Grothausmann, M. Dawson, C. Hartnig, S. Haas, D. Thomas, A. Hoell, C. Genzel, J. Banhart, Advanced Engineering Materials, 13 (2011) 712-729.
[8] M. Strobl, I. Manke, N. Kardjilov, A. Hilger, M. Dawson, J. Banhart, Journal of Physics D-Applied Physics, 42 (2009).
[9] M.A. Hickner, N.P. Siegel, K.S. Chen, D.N. McBrayer, D.S. Hussey, D.L. Jacobson, M. Arif, Journal of The Electrochemical Society, 153 (2006) A902-A908.
[10] P. Boillat, D. Kramer, B.C. Seyfang, G. Frei, E. Lehmann, G.G. Scherer, A. Wokaun, Y. Ichikawa, Y. Tasaki, K. Shinohara, Electrochemistry Communications, 10 (2008) 546-550.
[11] D.J. Ludlow, C.M. Calebrese, S.H. Yu, C.S. Dannehy, D.L. Jacobson, D.S. Hussey, M. Arif, M.K. Jensen, G.A. Eisman, Journal of Power Sources, 162 (2006) 271-278.
[12] A. Turhan, K. Heller, J.S. Brenizer, M.M. Mench, Journal of Power Sources, 160 (2006) 1195-1203.
[13] J.J. Kowal, A. Turhan, K. Heller, J. Brenizer, M.M. Mench, Journal of The Electrochemical Society, 153 (2006) A1971-A1978.
[14] D. Kramer, J. Zhang, R. Shimoi, E. Lehmann, A. Wokaun, K. Shinohara, G.G. Scherer, Electrochimica Acta, 50 (2005) 2603-2614.
[15] J. Zhang, D. Kramer, R. Shimoi, Y. Ono, E. Lehmann, A. Wokaun, K. Shinohara, G.G. Scherer, Electrochimica Acta, 51 (2006) 2715-2727.
[16] C. Hartnig, I. Manke, N. Kardjilov, A. Hilger, M. Grünerbel, J. Kaczerowski, J. Banhart, W. Lehnert, Journal of Power Sources, 176 (2008) 452-459.
[17] I. Manke, C. Hartnig, N. Kardjilov, M. Messerschmidt, A. Hilger, M. Strobl, W. Lehnert, J. Banhart, Applied Physics Letters, 92 (2008) 244101.
[18] M.A. Hickner, N.P. Siegel, K.S. Chen, D.S. Hussey, D.L. Jacobson, M. Arif, Journal of The Electrochemical Society, 155 (2008) B427-B434.
[19] A. Geiger, A. Tsukada, E. Lehmann, P. Vontobel, A. Wokaun, G. Scherer, Fuel Cells, 2 (2002) 92-98.
[20] R.J. Bellows, M.Y. Lin, M. Arif, A.K. Thompson, D. Jacobson, Journal of The Electrochemical Society, 146 (1999) 1099-1103.

[21] R. Satija, D.L. Jacobson, M. Arif, S.A. Werner, Journal of Power Sources, 129 (2004) 238-245.

[22] J.P. Owejan, T.A. Trabold, D.L. Jacobson, D.R. Baker, D.S. Hussey, M. Arif, International Journal of Heat and Mass Transfer, 49 (2006) 4721-4731.

[23] A. Schröder, K. Wippermann, J. Mergel, W. Lehnert, D. Stolten, T. Sanders, T. Baumhöfer, D.U. Sauer, I. Manke, N. Kardjilov, A. Hilger, J. Schloesser, J. Banhart, C. Hartnig, Electrochemistry Communications, 11 (2009) 1606-1609.

[24] A. Schröder, K. Wippermann, W. Lehnert, D. Stolten, T. Sanders, T. Baumhöfer, N. Kardjilov, A. Hilger, J. Banhart, I. Manke, Journal of Power Sources, 195 (2010) 4765-4771.

[25] C. Tötzke, I. Manke, A. Hilger, G. Choinka, N. Kardjilov, T. Arlt, H. Markötter, A. Schröder, K. Wippermann, D. Stolten, C. Hartnig, P. Krüger, R. Kuhn, J. Banhart, Journal of Power Sources, 196 (2011) 4631-4637.

[26] C. Hartnig, I. Manke, J. Schloesser, P. Krüger, R. Kuhn, H. Riesemeier, K. Wippermann, J. Banhart, Electrochemistry Communications, 11 (2009) 1559-1562.

[27] C. Hartnig, I. Manke, R. Kuhn, S. Kleinau, J. Goebbels, J. Banhart, Journal of Power Sources, 188 (2009) 468-474.

[28] I. Manke, C. Hartnig, M. Grunerbel, W. Lehnert, N. Kardjilov, A. Haibel, A. Hilger, J. Banhart, H. Riesemeier, Applied Physics Letters, 90 (2007) 174105.

[29] I. Manke, C. Hartnig, N. Kardjilov, H. Riesemeier, J. Goebbels, R. Kuhn, P. Krüger, J. Banhart, Fuel Cells, 10 (2010) 26-34.

[30] C. Hartnig, I. Manke, R. Kuhn, N. Kardjilov, J. Banhart, W. Lehnert, Applied Physics Letters, 92 (2008) 134106.

[31] S.J. Lee, N.-Y. Lim, S. Kim, G.-G. Park, C.-S. Kim, Journal of Power Sources, 185 (2008) 867-870.

[32] K.W. Feindel, S.H. Bergens, R.E. Wasylishen, Phys. Chem. Chem. Phys.,, 9 (2007) 1850 - 1857.

[33] K.W. Feindel, S.H. Bergens, R.E. Wasylishen, Journal of Power Sources, 173 (2007) 86-95.

[34] K.W. Feindel, S.H. Bergens, R.E. Wasylishen, Journal of the American Chemical Society, 128 (2006) 14192-14199.

[35] N. Kardjilov, A. Hilger, I. Manke, M. Strobl, M. Dawson, S. Williams, J. Banhart, Nuclear Instruments and Methods in Physics Research Section A: Accelerators, Spectrometers, Detectors and Associated Equipment, DOI: 10.1016/j.nima.2011.01.067, in press (2011).

[36] M. Strobl, A. Hilger, N. Kardjilov, I. Manke, W. Treimer, M. Riemke, Time-of-Flight Spectrum Measurements at the Neutron Imaging Facility CONRAD at the Hahn-Meitner Institute, 2008.

[37] P. Böni, Nuclear Instruments and Methods in Physics Research Section A: Accelerators, Spectrometers, Detectors and Associated Equipment, 586 (2008) 1-8.

[38] N. Kardjilov, A. Hilger, M. Dawson, I. Manke, J. Banhart , M. Strobl, P. Böni, Journal of Applied Physics 108 (2010) 034905.